# Density Functional Theory Investigation into the Mechanism for $\eta^2$-Alkyne to Vinylidene Isomerization by the Addition of Phenylacetylene to $[(\eta^3\text{-}C_3H_5)Rh(P\textit{i}Pr_3)_2]$

Benjamin Alan Vastine and Michael B. Hall*

*Department of Chemistry, Texas A&M University, College Station, Texas 77842*

*Received February 7, 2008*

The mechanism for the formation of the alkynyl, vinylidene complex $[(P\textit{i}Pr_3)_2Rh(CCPh)(CC(H)(Ph))]$ (**2**) by the addition of 2 equiv of phenylacetylene to $[(\eta^3\text{-}C_3H_5)Rh(P\textit{i}Pr_3)_2]$ (**1**) was studied through DFT calculations. At the B3LYP/DZP level of theory, the formation of **2** is exothermic and exergonic by 25.6 and 18.1 kcal·mol$^{-1}$, respectively. The experimentally observed $\eta^2$-phenyacetylene, alkynyl complex $[(P\textit{i}Pr_3)_2Rh(\eta^2\text{-}HCCPh)(CCPh)]$ (**Ia**), is exothermic and exergonic by 22.4 and 12.5 kcal·mol$^{-1}$, respectively. In the lowest energy pathway from **Ia** to **2**, the $\eta^2$-phenylacetylene of **Ia** slips to bind through the $\sigma$-C−H bond to form the intermediate $[(P\textit{i}Pr_3)_2Rh(\sigma\text{-}HCCPh)(CCPh)]$. Then, a single transition state (TS) ($\Delta H^{\ddagger} = 24.6$ kcal·mol$^{-1}$) connects this intermediate to **2**. In an alternative route, oxidative splitting of the $\sigma$-C−H bond results in the experimentally observed bis-alkynyl rhodium hydride complex $[(P\textit{i}Pr_3)_2Rh(H)(CCPh)_2]$ (**Ib**), which was observed experimentally to be in equilibrium with **Ia**. Species **Ib** is isoenthalpic with respect to **Ia** ($\Delta H°_{\text{Ib-Ia}} = -0.36$ kcal·mol$^{-1}$). A pathway was located for formation of **2** from **Ib**; however, the calculated barrier of 35.4 kcal·mol$^{-1}$ is too high for this pathway to be viable. This alternative pathway seems to be the lowest energy pathway for the chloro analogue $[ClRh(P\textit{i}Pr_3)_2(\eta^2\text{-}HCCPh)]$ (**Ia-Cl**). Here, the $\sigma$-bound phenylacetylene complex was not located; instead, the first transition state results in oxidative cleavage of the $\sigma$-C−H bond to form the analogue of **Ib**, $[ClRh(P\textit{i}Pr_3)_2(H)(CCPh)]$ (**Ib-Cl**). A single transition state connects this species with the vinylidene product $[ClRh(P\textit{i}Pr_3)_2(CC(H)(Ph))]$ (**2-Cl**). The barrier for hydrogen migration in this pathway is 25.4 kcal·mol$^{-1}$. The phenylacetylide ligand stabilizes the $\sigma$-binding mode of the second phenylacetylene; as a result, the mechanism for vinylidene formation from **Ia** is altered slightly from the common *1−3 shift* mechanism operating for the analogue **Ia-Cl**.

## Introduction

Hydrocarbons can have "ubiquitous functionality" with well-developed techniques for facile carbon−hydrogen (C−H) bond activation.[1] Facile activation of this bond can occur at transition metals (TM),[2] and selectivity has been demonstrated with TM systems.[3] For example, the isomerization of an alkyne to the corresponding vinylidene (HCCX → :CC(H)(X)), which in the gas phase is very endothermic,[4] can be easily accomplished at a TM center.[5]

Werner and co-workers studied this isomerization from $[ClRh(P\textit{i}Pr_3)_2(\eta^2\text{-}HCCH)]$ to form the vinylidene product $[C_5H_5Rh(P\textit{i}Pr_3)(CCH_2)]$ (upon ligand exchange and phosphine loss).[6] An oxidative pathway for this isomerization was proposed as analogues of the $\eta^2$-alkyne reactant, the alkynyl rhodium hydride complex, and the vinylidene product were isolated with phenylacetylene.[7] Analogues of these species were also isolated with iridium, which further supported the oxidative pathway.[8]

Wakatsuki et al. theoretically studied the oxidative pathway from the reactant $[ClRh(PH_3)_2(\eta^2\text{-}HCCH')]$ and found that this pathway proceeded in two steps (Scheme 1, [Rh] = ClRh-$(PH_3)_2$).[9a] Oxidative cleavage of acetylene from the reactant to form the five-coordinate, alkynyl rhodium hydride intermediate $[ClRh(PH_3)_2(H)(CCH')]$ was the first step. In the second step, the vinylidene product $[ClRh(PH_3)_2(CC(H)(H'))]$ was formed from hydrogen migration from the rhodium to the $\beta$-carbon. A single TS between the alkynyl rhodium hydride intermediate and the vinylidene product was found and characterized as an inverted "T-shaped" geometry. However, the barrier for this so-called *1−3 shift* pathway was high (∼34 kcal·mol$^{-1}$), and a bimolecular mechanism was investigated and found to be lower in energy than the former. Subsequently, Stegmann and Frenking found a *1−3 shift* pathway in a study on the rearrangement on W.[9b]

**Scheme 1**

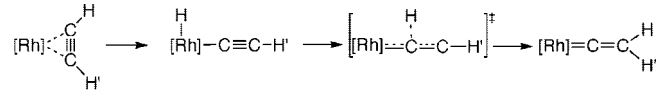


Grotjahn et al. reported that H/D crossover was not observed when the complexes $[ClRh(P\textit{i}Pr_2R^1)_2(\eta^2\text{-}HCC\textit{i}Pr)]$ ($R^1$ = Ph, *i*Pr, imidazol-2-yl) and deuterated alkyne analogues were mixed.[10] Thus, the bimolecular pathway was eliminated as the mechanism for this isomerization. In further work, these researchers confirmed the *1−3 shift* mechanism.[11] In a more recent computational study, De Angelis et al. investigated this

* Corresponding author. E-mail: hall@science.tamu.edu.

(1) Godula, K.; Sames, D. *Science* **2006**, *312*, 67–72.
(2) Shilov, A. E.; Shul'pin, G. B. *Chem. Rev.* **1997**, *97*, 2879–2932.
(3) (a) Green, M. L. H.; Knowles, P. J. *J. Chem. Soc., Chem. Commun.* **1970**, 1677. (b) Hoyano, J. K.; Graham, W. A. G. *J. Am. Chem. Soc.* **1982**, *104*, 3723–3725. (c) Janowicz, A. H.; Bergman, R. G. *J. Am. Chem. Soc.* **1982**, *104*, 352–354.
(4) (a) Chen, Y.; Jonas, D. M.; Kinsey, J. L.; Field, R. W. *J. Chem. Phys.* **1989**, *91*, 3976–3987. (b) Ervin, K. M.; Ho, J.; Lineberger, W. C. *J. Chem. Phys.* **1989**, *91*, 5974–5992.

10.1021/om8001137 CCC: $40.75 
Publication on Web 08/14/2008

**Scheme 2**

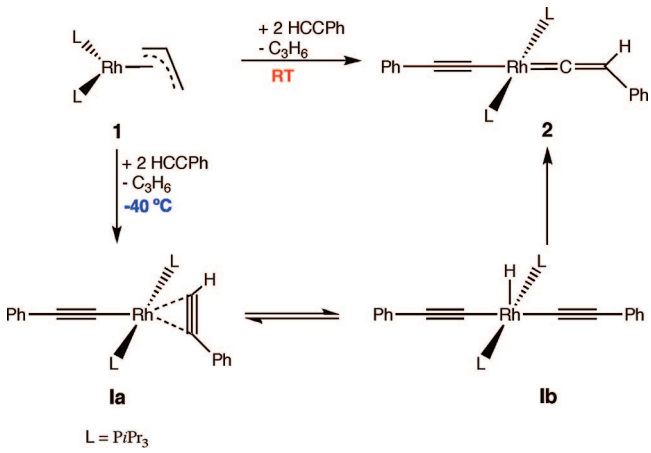


chemistry for the starting material (SM) [ClRh(P*i*Pr$_3$)$_2$($\eta^2$-HCCH)] and found that the enthalpic barriers to hydrogen migration in the intra- and bimolecular pathways were similar, but the free energy barrier of the intramolecular pathway was ~20 kcal·mol$^{-1}$ less than that of the bimolecular pathway.[12]

In further studies of this isomerization, Werner and co-workers added 2 equiv of phenylacetylene (HCCPh) to [($\eta^3$-C$_3$H$_5$)Rh(P*i*Pr$_3$)$_2$] (**1**) to form the alkynyl, vinylidene rhodium product **2** and proposed the sequence shown in Scheme 2.[13] At room temperature (RT), the reaction proceeded to the alkynyl, vinylidene complex **2**; however, at −40 °C, the reaction proceeded to the $\pi$-bound phenylacetylene, alkynyl complex **Ia**. In solution, **Ia** was observed (via $^1$H NMR) to be in equilibrium with **Ib**, the bis-alkynyl rhodium hydride complex. Complex **Ib** was trapped by running the reaction in excess pyridine, where a pyridine molecule coordinated *trans* to the hydride to form **Ib**(pyr). These workers concluded that **Ia** and **Ib** are intermediates on the reaction pathway that results in the formation of **2**, as shown in Scheme 2.

Here, the mechanism for the formation of **2** was examined by density functional theory[14] (DFT). The issues addressed include the effect of the phosphine on the relative energies (section 1), the pathway to form **Ia** (section 2), three alternative pathways for the alkyne (**Ia**) to vinylidene (**2**) isomerization (section 3), and the difference between the phenylacetylene system and the chloro analogue.

## Computational Method

All DFT calculations reported here were performed with the Gaussian03[15] suite of programs. Each complex reported in this section was optimized at the B3LYP/BS1 level of theory, and the analytical frequencies were calculated to determine if the force constants were real (intermediate) or if one was imaginary (TS). The default convergence criteria were used for all optimizations. The B3LYP density functional is a combination of the Becke3 exchange[16] and Lee−Yang−Parr correlation[17] functionals. Basis set 1 (BS1) is defined as follows: Rhodium was assigned the small-core Los Alamos National Laboratory 2 (LANL2) effective core potential of Hay and Wadt[18] and the valence double-$\zeta$ (341/341/31) basis set as modified by Couty and Hall (ECP/BS = LANL2mDZ);[19] the phosphorus, C$_\alpha$, C$_\beta$, C$_\gamma$, C$_1'$, C$_1''$, C$_2'$, C$_2''$, H′, and H″ atoms were assigned the correlation consistent polarized valence double-$\zeta$ (cc-pVDZ) basis sets of Dunning;[20] the remaining carbon and hydrogen atoms were assigned the full double-$\zeta$ (D95) basis sets of Dunning.[21] For the B3LYP/BS1-optimized intermediates and TSs, frequency calculations were performed at this same level of theory from which the zero-point correction and corrections to the electronic energy, enthalpy, and free energy were obtained.

For the barriers for allyl rearrangement that were refined at a higher level of theory (**TS$_{1-3}$**, **TS′**), the basis set used (BSr) consists of the Stuttgart relativistic small-core (RSC) 1997 ECP and the triple-$\zeta$ basis set.[22] The phosphorus, C$_\alpha$, C$_\beta$, and C$_\gamma$ atoms were assigned the correlation consistent polarized valence triple-$\zeta$ (cc-pVTZ) basis sets of Dunning,[20] and the remaining carbon and hydrogen atoms retained the original assignments of the D95 basis sets.[21] The B3LYP/BSr//B3LYP/BS1 energies were corrected with the B3LYP/BS1 corrections to the enthalpy and free energy to obtain the thermodynamic values for these barriers.

The values discussed in the text are primarily enthalpies ($\Delta H^{\circ/\ddagger}$) and free energies ($\Delta G^{\circ/\ddagger}$) in the gas phase at standard

(5) (a) Nesmeyanov, A. N.; Aleksandrov, G. G.; Antonova, A. B.; Anisimov, K. N.; Kolobova, N. E.; Struchkov, Yu. T. *J. Organomet. Chem.* **1976**, *110*, C36–C38. (b) Antonova, A. B.; Kolobova, N. E.; Petrovsky, P. V.; Lokshin, B. V.; Obezyuk, N. S. *J. Organomet. Chem.* **1977**, *137*, 55–67. (c) Kolobova, N. E.; Antonova, A. B.; Khitrova, O. M.; Antipin, M. Yu.; Struchkov, Yu. T. *J. Organomet. Chem.* **1977**, *110*, 69–78. (d) Silvestre, J.; Hoffmann, R. *Helv. Chim. Acta* **1985**, *68*, 1461–1506. (e) De Angelis, F.; Fantacci, S.; Sgamellotti, A. *Coord. Chem. Rev.* **2006**, *250*, 1497–1513. (f) Selegue, J. P. *Organometallics* **1982**, *1*, 217–218. (g) De Angelis, F.; Sgamellotti, A.; Re, N. *Organometallics* **2002**, *21*, 5944–5950. (h) De Angelis, F.; Sgamellotti, A.; Re, N. *Dalton Trans.* **2004**, 3225–3230. (i) Olivan, M.; Clot, E.; Eisenstein, O.; Caulton, K. G. *Organometallics* **1998**, *17*, 3091–3100. (j) Clot, E.; Eisenstein, O. Chapter 6: Isomerization of Double and Triple C-C Bonds at a Metal Center. In *Computational Modeling of Homogeneous Catalysis*; Maseras, F., Lledós, A., Eds.; Kluwer Academic Publishers: Dordrecht, 2002.

(6) Wolf, J.; Werner, H.; Serhadli, O.; Ziegler, M. L. *Angew. Chem., Int. Ed. Engl.* **1983**, *22*, 414–416.

(7) Werner, H.; Wolf, J.; Garcia Alonso, F. J.; Ziegler, M. L.; Serhadli, O. *J. Organomet. Chem.* **1987**, *336*, 397–411.

(8) Garcia Alonso, F. J.; Hohn, A.; Wolf, J.; Otto, H.; Werner, H. *Angew. Chem., Int. Ed. Engl.* **1985**, *24*, 406–407.

(9) (a) Wakatsuki, Y.; Koga, N.; Werner, H.; Morokuma, K. *J. Am. Chem. Soc.* **1997**, *119*, 360–366. (b) Stegmann, R.; Frenking, G. *Organometallics* **1998**, *17*, 2089–2095.

(10) Grotjahn, D. B.; Zeng, X.; Cooksy, A. L. *J. Am. Chem. Soc.* **2006**, *128*, 2798–2799.

(11) Grotjahn, D. B.; Zeng, X.; Cooksy, A. L.; Kassel, W. S.; DiPasquale, A. G.; Zakharov, L. N.; Rheingold, A. L. *Organometallics* **2007**, *26*, 3385–3402.

(12) De Angelis, F.; Sgamellotti, A.; Re, N. *Organometallics* **2007**, *26*, 5285–5288.

(13) Schäfer, M.; Wolf, J.; Werner, H. *Organometallics* **2004**, *23*, 5713–5728.

(14) Parr, R. G.; Yang, W. In *Density Functional Theory of Atoms and Molecules*; Oxford University Press: New York, 1989; pp 1−333.

(15) Frisch, M. J. ; Trucks, G. W.; Schlegel, H. B.; Scuseria, G. E.; Robb, M. A.; Cheeseman, J. R.; Montgomery, J. A., Jr.; Vreven, T.; Kudin, K. N., Burant, J. C.; Millam, J. M.; Iyengar, S. S.; Tomasi, J.; Barone, V.; Mennucci, B.; Cossi, M.; Scalmani, G.; Rega, N.; Petersson, G. A.; Nakatsuji, H.; Hada, M.; Ehara, M.; Toyota, K.; Fukuda, R.; Hasegawa, J.; Ishida, M.; Nakajima, T.; Honda, Y., Kitao, O.; Nakai, H.; Klene, M.; Li, X.; Knox, J. E.; Hratchian, H. P.; Cross, J. B.; Bakken, V.; Adamo, C.; Jaramillo, J.; Gomperts, R.; Stratmann, R. E.; Yazyev, O.; Austin, A. J.; Cammi, R.; Pomelli, C.; Ochterski, J. W.; Ayala, P. Y.; Morokuma, K.; Voth, G. A.; Salvador, P.; Dannenberg, J. J.; Zakrzewski, V. G.; Dapprich, S.; Daniels, A. D.; Strain, M. C.; Farkas, O.; Malick, D. K.; Rabuck, A. D.; Raghavachari, K.; Foresman, J. B.; Ortiz, J. V.; Cui, Q.; Baboul, A. G.; Clifford, S.; Cioslowski, J.; Stefanov, B. B.; Liu, G.; Liashenko, A.; Piskorz, P.; Komaromi, I.; Martin, R. L.; Fox, D. J.; Keith, T.; Al-Laham, M. A.; Peng, C. Y.; Nanayakkara, A.; Challacombe, M.; Gill, P. M. W.; Johnson, B.; Chen, W.; Wong, M. W.; Gonzalez, C.; Pople, J. A. *Gaussian 03*, Revision D.02; Gaussian, Inc.: Wallingford, CT, 2004.

(16) Becke, A. D. *J. Chem. Phys.* **1993**, *98*, 5648–5652.

(17) Lee, C.; Yang, W.; Parr, R. G. *Phys. Rev. B: Condens. Matter Mater. Phys.* **1988**, *37*, 785–789.

(18) Hay, P. J.; Wadt, W. R. *J. Chem. Phys.* **1985**, *82*, 270–283.

(19) Couty, M.; Hall, M. B. *J. Comput. Chem.* **1996**, *17*, 1359–370.

(20) (a) Dunning, T. H. *J. Chem. Phys.* **1989**, *90*, 1007–1023. (b) Woon, D. E.; Dunning, T. H., Jr. *J. Chem. Phys.* **1993**, *98*, 1358–1371.

(21) Dunning, T. H.; Hay, P. J. *Modern Theoretical Chemistry*; Schaefer, H. F., III, Ed.; Plenum: New York; 1976; pp 1−28.

(22) Kaupp, M.; Schleyer, P. v. R.; Stoll, H.; Preuss, H. *J. Chem. Phys.* **1991**, *94*, 1360–1366.

**Table 1. Relative Energies of Ia, Ib, and 2 (energies are relative to 1 + 2HCCPh, reported in kcal·mol$^{-1}$)**

| | 1 | | 2 | | Ia | | Ib | |
|---|---|---|---|---|---|---|---|---|
| | $\Delta H°$ | $\Delta G°$ | $\Delta H°$ | $\Delta G°$ | $\Delta H°$ | $\Delta G°$ | $\Delta H°$ | $\Delta G°$ |
| P*i*Pr$_3$[a] | 0 | 0 | −25.41 | −15.54 | −23.76 | −12.99 | −21.81 | −13.49 |
| P*i*Pr$_3$[b] | | | −27.67 | −17.33 | −24.17 | −13.92 | −25.32 | −17.41 |
| P*i*Pr$_3$[c] | | | −25.60 | −18.10 | −22.43 | −12.51 | −22.79 | −16.60 |
| PEt$_3$ | | | −17.57 | −7.98 | −17.08 | −6.33 | −14.61 | −5.69 |
| PMe$_3$ | | | −17.01 | −8.29 | −18.46 | −8.59 | −13.25 | −4.94 |
| PMe$_2$Ph | | | −13.17 | −3.79 | −14.70 | −5.85 | −10.26 | −0.71 |
| PMePh$_2$ | | | −12.45 | −2.23 | −14.46 | −3.36 | −7.89 | 2.68 |
| PPh$_3$ | | | −15.30 | −7.80 | −17.65 | −8.51 | −10.47 | 1.38 |
| PH$_3$ | | | −6.93 | 3.70 | −10.51 | 0.36 | 2.03 | 9.85 |
| PCl$_3$ | | | 11.57 | 23.29 | 2.94 | 12.06 | 27.04 | 36.17 |
| PF$_3$ | | | 12.39 | 21.75 | 5.34 | 12.92 | 28.93 | 38.48 |

[a] "Chase" arrangement. [b] "Umbrella" arrangement. [c] Crystal structure alignment.

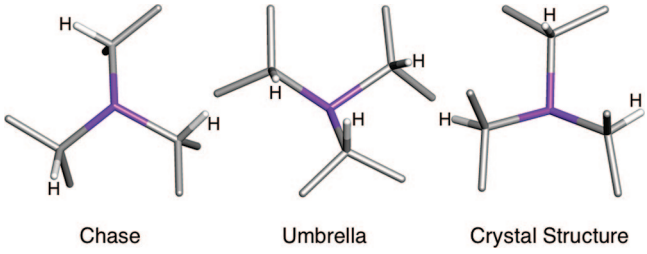


**Figure 1.** The three arrangements of the P*i*Pr$_3$ ligand that are used in this study. The methyl hydrogen atoms have been removed for clarity.

conditions (298 K, 1 atm). The electronic energies ($\Delta E_{elec}$), electronic energies with zero-point corrections ($\Delta E_0$), enthalpies ($\Delta H°^{/\ddagger}$), and free energies ($\Delta G°^{/\ddagger}$) are reported in the tables. All 3D representations of the optimized molecular geometries were constructed with JIMP 2.[23]

## Results and Discussion

**Effect of Phosphine Ligand on Relative Energies.** The relative energies of **Ia**, **Ib**, and **2** (all relative to **1** + 2HCCPh) were calculated with a variety of phosphines, and the results are presented in Table 1. Three arrangements of P*i*Pr$_3$ are examined and illustrated in Figure 1. For "chase" arrangement, the primary carbon atoms of the individual propyl units reside above and below the Rh−C−H plane, and rotation about the "$C_3$" axis will turn each propyl unit into the other (highest point group $C_3$). For "umbrella" arrangement, the hydrogen atoms of each secondary carbon are pointed toward the center of the phosphine (highest point group $C_{3v}$). For the crystal structure arrangement, two of the propyl units are related by a mirror plane with the hydrogen atoms pointed away from each other, while the third propyl unit is rotated 120° about the Rh−C bond relative to the other propyl units (highest point group $C_s$). The former two forms are higher in energy than the latter by 11.7 and 18.4 kcal·mol$^{-1}$, respectively.

For a given P*i*Pr3 arrangement, the energetic results for **2**, **Ia**, and **Ib** are quite similar; **2** is the most stable, while **Ia** and **Ib** are of similar stabilities. Interestingly, the enthalpies of **Ia** and **Ib** are closest for the observed arrangement. On the other hand, the results for smaller phosphines are quite different. Species **2** was the predicted product for P*i*Pr$_3$ and PEt$_3$, while **Ia** was the predicted product with other phosphines from PMe$_3$ to PH$_3$, while the reaction was endothermic with PF$_3$ and PCl$_3$. Even PEt$_3$ does not show the strong enthalpic preference for **2** over **Ia** that is shown for P*i*Pr$_3$.We used the crystal structure form of P*i*Pr$_3$ in our study of the mechanism (sections 2 and 3).

**Table 2. Relative Energies for the Intermediates and TSs of Section 2 (energies are reported in kcal·mol$^{-1}$)**

| | set 1: relative to **1**[a] | | set 2: relative to prior intermediate[b] | |
|---|---|---|---|---|
| species | $\Delta H°^{/\ddagger}$ | $\Delta G°^{/\ddagger}$ | $\Delta H°^{/\ddagger}$ | $\Delta G°^{/\ddagger}$ |
| **1**[c] | 0 | 0 | 0 | 0 |
| **TS$_{1-3}$**[c] | 23.79 | 21.01 | 23.79 | 21.01 |
| **3**[c] | 19.49 | 14.46 | 19.49 | 14.46 |
| **4a**[d] | 11.94 | 23.55 | −7.55 | 9.08 |
| **4b** | 13.19 | 23.69 | −6.30 | 9.23 |
| **TS$_{4a-5a}$**[d] | 24.67 | 34.82 | 12.26 | 12.50 |
| **TS$_{4b-5b}$**[d] | 24.22 | 34.07 | 11.03 | 10.38 |
| **5a**[d] | 15.39 | 24.38 | 3.45 | 0.83 |
| **5b**[d] | 13.15 | 22.06 | −0.04 | −1.63 |
| **TS$_{5a-6a}$**[d] | 16.89 | 26.09 | 1.50 | 1.72 |
| **TS$_{5b-6b}$**[d] | 14.42 | 22.83 | 1.27 | 0.77 |
| **6a**[d] | 7.25 | 17.19 | −8.14 | −7.18 |
| **6b**[d] | 7.21 | 15.70 | −5.95 | −6.36 |
| **TS$_{6a-8}$**[d] | 11.98 | 21.59 | 4.73 | 4.40 |
| **TS$_{6b-7b}$**[d] | 10.91 | 19.44 | 3.70 | 3.74 |
| **7a**[d] | NA | NA | NA | NA |
| **7b**[d] | −2.98 | 1.16 | −10.19 | −14.55 |
| **8**[e] | −5.86 | −13.27 | | |
| **9**[f] | −12.85 | −2.44 | | |
| **Ia**[g] | −22.43 | −12.51 | | |

[a] Relative to **1** + 2HCCPh. [b] IM; TS is relative to preceding IM. [c] +2HCCPh. [d] + HCCPh. [e] +HCCPh, $C_3H_6$. [f] +HCCPh. [g] +$C_3H_6$.

**Mechanism for the Formation of Ia.** In this section, we present our calculated mechanism for the addition of 2 equiv of HCCPh to **1** to form the intermediate **Ia**. The formation of this intermediate follows the isomerization of **1**, the binding and activation of the first equivalent of HCCPh, the elimination of propene, and finally the binding of the second equivalent of HCCPh. For the allyl ligand, the three carbons are labeled $C_\alpha$, $C_\beta$, and $C_\gamma$. In the first equivalent of HCCPh, the sp carbon atoms are labeled $C_1'$ and $C_2'$, and the transferring hydrogen is labeled H′. The relative enthalpies and free energies for the intermediates and TSs on this pathway are presented in Table 2, where values are presented as relative to **1** (+ 2HCCPh) in the first set and relative to the intermediate that precedes the following TS and next intermediate in the second set. For example, the numbers reported for both **TS$_{4a-5a}$** and **5a** in the second set are relative to **4a**. The optimized geometries of **1** through **9** are included in the Supporting Information.

**Isomerization of the Reactant.** Two plausible mechanisms for the isomerization of **1** are considered (Scheme 3). Complex **1** exists as a pseudo-square-planar, four-coordinate $\eta^3$-allyl Rh$^{I}$

(23) (a) Manson, J.; Webster, C. E.; Pérez, L. M.; Hall, M. B. *JIMP 2 Version 0.091 (built for Windows PC)*; Department of Chemistry, Texas A&M University: College Station, TX, 2006 (available at http://www.chem.tamu.edu/jimp2/index.html)(b) Hall, M. B.; Fenske, R. F. *Inorg. Chem.* **1972**, *11*, 768–779.

(24) Werner, H. *J. Organomet. Chem.* **1994**, *475*, 45–55.

**Scheme 3**

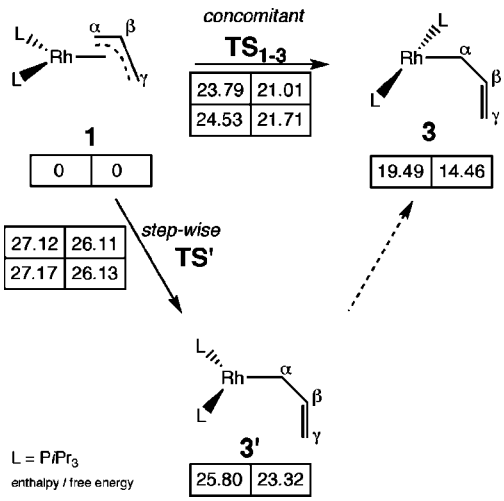


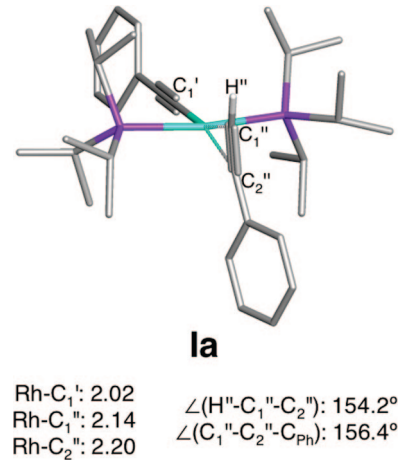


**Figure 2.** B3LYP/BS1-optimized geometry **Ia** and select optimized parameters. Distances listed are in angstroms and angles in degrees. Nonessential hydrogen atoms have been removed for clarity.

**Scheme 4**

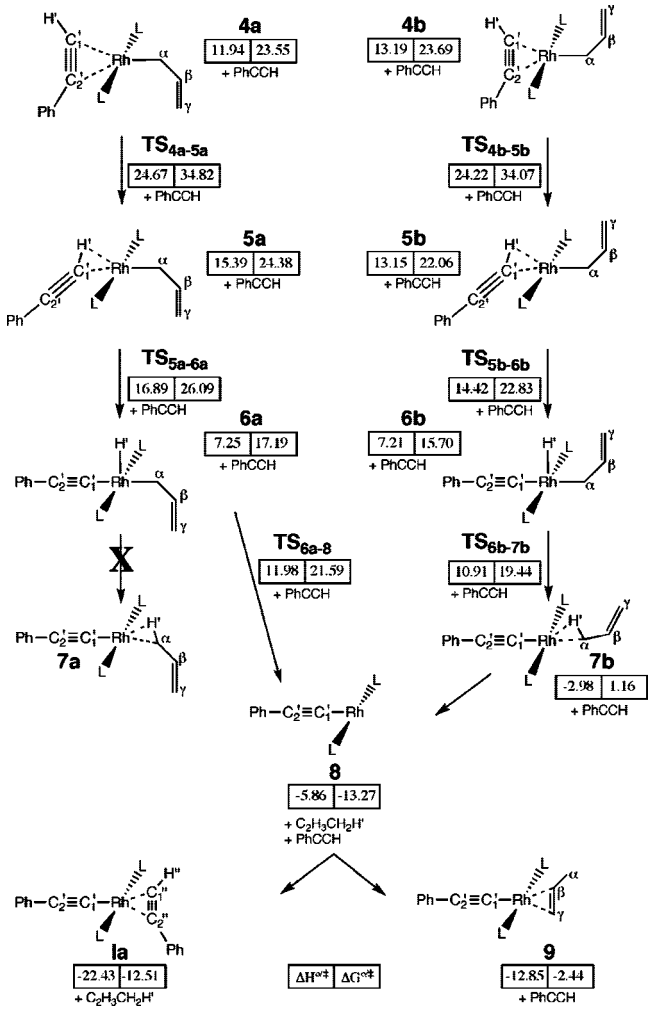


complex with $C_\alpha-Rh-C_\gamma$ and P−Rh−P angles of 66.7° and 109.4°, respectively. In complex **3**, the allyl has slipped to bind $\eta^1$ to the rhodium and results in a pseudo-T-shaped, three-coordinate, $\eta^1$-allyl $Rh^I$ complex with a P−Rh−P angle of 165.1°. This isomerization opens a coordinate site for the binding of the first equivalent of phenylacetylene. Complexes **1** and **3** are joined by a single TS (**$TS_{1-3}$**) where, in the animation of the imaginary mode, the widening of the P−Rh−P angle is *concomitant* with allyl slippage. At the B3LYP/BS1 level of theory, the enthalpic and free energy barriers to this isomerization are 23.8 and 21.0 kcal·mol$^{-1}$, respectively.

A *stepwise* mechanism for this isomerization was also investigated, but it proceeds through a higher energy intermediate (**3′**). Mechanistically, the allyl slips to $\eta^1$ prior to a change in the P−Rh−P angle, which in **3′** is nearly identical to that of **1** (110.7°). A transition state (**TS′**) was located that connects **1** to **3′** where, in the animation of the imaginary mode, the allyl slips to bind $\eta^1$ without a significant change in the P−Rh−P angle. At the B3LYP/BS1 level of theory, the enthalpic and free energy barriers of this *stepwise* pathway (**TS′**) are 27.2 and 26.1 kcal·mol$^{-1}$, respectively, which are 3.3 and 5.1 kcal·mol$^{-1}$ greater than those of the *concomitant* pathway.

The enthalpic and free energy barriers of **$TS_{1-3}$** and **TS′** were refined at the higher level in the basis (B3LYP/BSr) and reported in the second row of the 2 × 2 boxes in Scheme 3. The enthalpic and free energy barriers for the *concomitant* pathway are slightly higher at this level of theory, but the values for the *stepwise* pathway are nearly identical. As a result, the enthalpic and free energy barriers of **TS′** are greater than **$TS_{1-3}$** by 2.6 and 4.4 kcal·mol$^{-1}$, respectively; therefore, the *stepwise* pathway was not pursued further.

**Binding of First Equivalent of HCCPh.** The binding of the first equivalent of HCCPh to **3** would follow the isomerization of **1** and may assist it in ways not examined here. Scheme 4 shows the pathways in the reactions from here (HCCPh + **3**) to the formation of **Ia**. The enthalpies and free energies (relative to **1** + 2(HCCPh)) are reported in kcal·mol$^{-1}$ and included in the scheme. Isomer **4a** is a pseudo-square-planar, $Rh^I$ complex where the $\eta^1$-allyl is aligned *syn* to the phenyl ring of the $\eta^2$-HCCPh, while complex **4b** is a rotormer of **4a** where the allyl has rotated ∼180° around the $Rh-C_\alpha$ bond to align *anti* to the HCCPh ligand (**a** and **b** will be used to designate these two types of isomers when a distinction is important). This rotation causes few changes in most of the geometric parameters; however, the $Rh-C_\alpha-C_\beta$ angle of **4b** is ∼17° wider than **4a**. These two rotamers are essentially isoenergetic; however, **4a** is more endothermic than **4b** by ∼5 kcal mol$^{-1}$. The $\pi$-binding of HCCPh stabilizes **4** by ∼7 kcal·mol$^{-1}$ ($\Delta H°_{\mathbf{4a(b)\text{-}3}}$) but is endergonic by ∼9 kcal·mol$^{-1}$. In both isomers of **4**, the phenyl ring of the $\eta^2$-HCCPh ligand is orthogonal to the Rh−P axes.

**Isomerization from the $\pi$- to $\sigma$-Binding Mode of HCCPh.** The $\eta^2$-phenylacetylene in **4** slips to bind through the $\sigma$-C−H bond, which results in **5**. The enthalpic difference ($\Delta H°$:

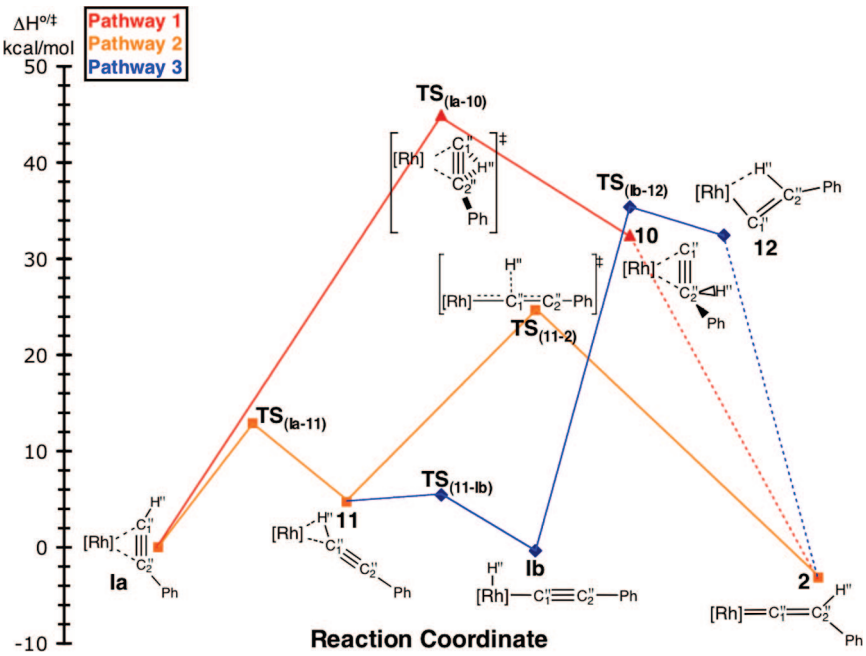


**Figure 3.** The three pathways for hydrogen transfer in the alkyne-to-vinylidene isomerization. Energies are relative to **Ia** and reported in kcal·mol$^{-1}$.

**Table 3. Relative Enthalpies and Free Energies of the Species along the Three Pathways for Alkyne-to-Vinylidene Isomerization (energies are relative to Ia and are reported in kcal·mol$^{-1}$)**

| pathway | species | $\Delta H^{\circ/\ddagger}$ | $\Delta G^{\circ/\ddagger}$ |
|---|---|---|---|
| | **Ia** | 0 | 0 |
| 1 | $\mathbf{TS_{Ia\text{-}10}}$ | 44.93 | 45.33 |
| | **10** | 32.13 | 30.14 |
| 2 | $\mathbf{TS_{Ia\text{-}11}}$ | 12.94 | 12.12 |
| | **11** | 4.71 | 1.68 |
| | $\mathbf{TS_{11-2}}$ | 24.64 | 25.54 |
| 3 | $\mathbf{TS_{11-Ib}}$ | 5.44 | 2.07 |
| | **Ib** | −0.36 | −4.09 |
| | $\mathbf{TS_{Ib\text{-}12}}$ | 35.39 | 34.54 |
| | **12** | 32.46 | 30.11 |
| | **2** | −3.16 | −5.59 |

**5** − **4**) for the **a** isomers is greater than that for the nearly isenthalpic **b** isomers; however, the free energy difference ($\Delta G^\circ$: **5** − **4**) between both pairs is small and opposite in sign. In the $\sigma$-binding mode, the phenyl ring of the HCCPh ligand has rotated roughly 90° to align parallel with the Rh−P axes.

Relative to **4**, the enthalpic and free energy barriers of the transition states ($\mathbf{TS_{4-5}}$) for this isomerization are greater than 10 kcal·mol$^{-1}$. Although one might expect a large steric influence on the barriers, calculations with $PMe_3$ and acetylene show even higher relative enthalpic and free energy barriers.

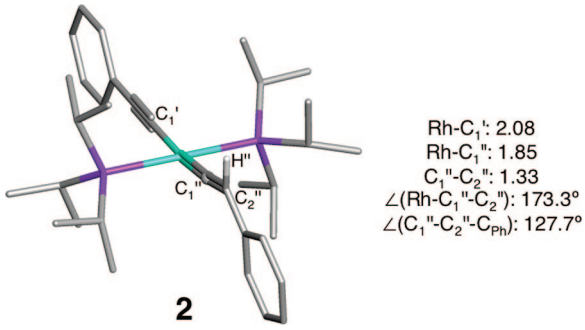


**Figure 4.** B3LYP/BS1-optimized geometry of **2** and select optimized parameters. Distances listed are in angstroms and angles in degrees. Nonessential hydrogen atoms have been removed for clarity.

The enthalpic barrier to isomerization between the two binding modes of HCCPh is calculated to be higher than the enthalpic barrier for the loss of HCCPh. Thus, the incoming HCCPh can bind in either the $\pi$- or $\sigma$-binding mode and freely decoordinate to rebind in either mode without proceeding through $\mathbf{TS_{4-5}}$.

**Oxidative Cleavage of the $C_1'$−H′ Bond.** The five-coordinate alkynyl rhodium hydride complexes **6a** and **6b** result from oxidative cleavage of the $C_1'$−H′ bond. The Rh−H′ bond lengths of these species (1.51 Å) are typical for a metal−hydride bond. Relative to the respective isomers of **5**, the formation of these intermediates are exothermic and exergonic by ∼8 and ∼6 kcal·mol$^{-1}$; these species are the last high-energy intermediates on the reaction coordinate. Relative to their respective isomers of **5**, the enthalpic and free energy barriers ($\mathbf{TS_{5-6}}$) to $C_1'$−H′ activation are small at ∼1 kcal·mol$^{-1}$.

**Reductive Coupling of the $C_\alpha$−H′ Bond.** Propene is formed by the reductive coupling of the $C_\alpha$−H′ bond, and relative to the respective isomers of **6**, the barriers ($\mathbf{TS_{6-8/7b}}$) to this coupling are small. This coupling in **6a** results in the direct elimination of propene and formation of the three-coordinate $Rh^I$ intermediate **8**, which is exothermic and exergonic by ∼13 and ∼30 kcal·mol$^{-1}$, respectively. Because the allyl is rotated away from the ligand sphere in the "**b**" isomers, coupling results in the pseudo-four-coordinate $Rh^I$ complex **7b**, in which propene remains bound to the rhodium. The corresponding isomer **7a** was not located on the B3LYP/BS1 potential energy surface (PES). The pseudo-four-coordinate $Rh^I$ complex **7b** is a higher energy intermediate than **8** but easily loses propene to form **8**.

**Formation of Ia.** After the formation of **8**, propene can recoordinate and $\pi$-bind to the rhodium to form **9**, or the second equivalent of HCCPh can $\pi$-bind to the rhodium to form **Ia**. The $\pi$-binding of HCCPh is more exothermic than the analogous binding of propene by ∼10 kcal·mol$^{-1}$. In terms of free energy, **Ia** is nearly isoenergetic with **8**, while **9** is endergonic by ∼10 kcal·mol$^{-1}$. Thus, **9** will not effect the overall reaction to any degree. The optimized geometry of **Ia** is shown in Figure 2.

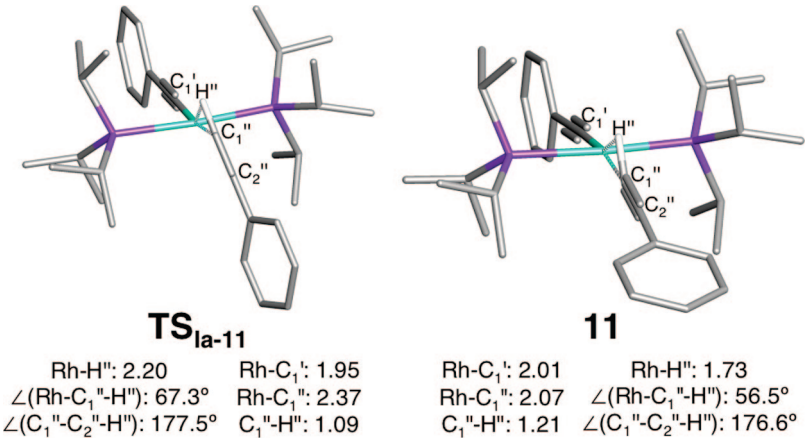


**Figure 5.** B3LYP/BS1-optimized geometry and select optimized parameters of $\mathbf{TS_{Ia\text{-}11}}$ and **11**. Distances listed are in angstroms and angles in degrees. Nonessential hydrogen atoms have been removed for clarity.

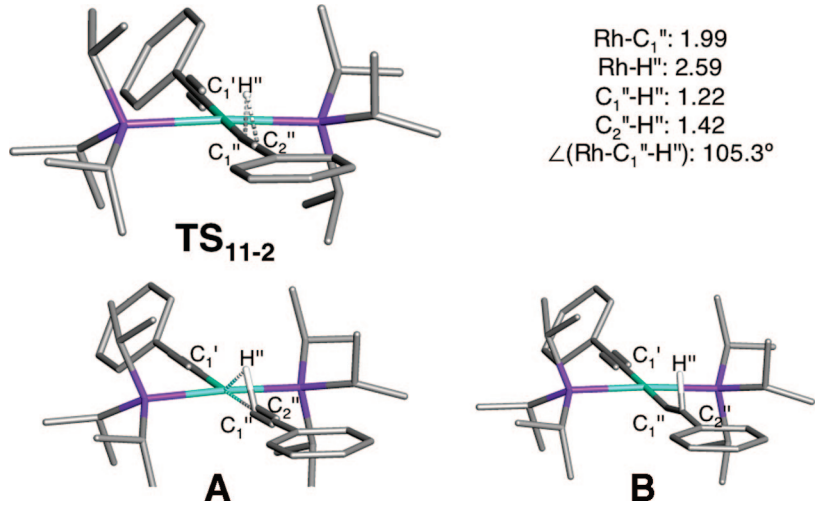


**Figure 6.** Optimized coordinates of $\mathbf{TS_{11-2}}$ and the two species from the IRC calculation. **A** is the result of hydrogen migration toward rhodium, and **B** is hydrogen migration toward $C_2$. Distances listed are in angstroms and angles in degrees.

**Phenylacetylene-to-Vinylidene Isomerization.** Three possible pathways for the formation of **2** from **Ia** are shown in Figure 3, and the relative enthalpies and free energies are given in Table 3 (relative to **Ia**). For the second equivalent of HCCPh, the sp carbon atoms are labeled $C_1''$ and $C_2''$, and the transferring hydrogen is labeled H″. The results for cobalt and iridium congeners of these rhodium species are reported in the Supporting Information.

The result of hydrogen migration is the vinylidene product **2**, where the optimized geometry is shown in Figure 4. The Rh−$C_1''$ bond length is short at 1.85 Å, which indicates that the vinylidene is tightly bound to the rhodium. The vinylidene is bent slightly as the Rh−$C_1''$−$C_2''$ angle is 173°. Relative to **Ia**, the formation of **2** is exothermic and exergonic by 3.2 and 5.6 kcal·mol$^{-1}$, respectively.

**Pathway 1.** In the first pathway (red curve), H″ migrates to $C_2''$ without a change in the geometry of the $\eta^2$-alkyne. In $\mathbf{TS_{Ia\text{-}10}}$, the migrating hydrogen is located orthogonal to the Rh−$C_1''$−$C_2''$ plane and the Rh−$C_1'$, Rh−$C_1''$, and Rh−$C_2''$ distances are similar to those of **Ia**. The enthalpic barrier in this pathway is large at ∼45 kcal·mol$^{-1}$, and the intermediate formed, **10**, the $\pi$-bound vinylidene rhodium complex, is unstable. Because of this high barrier, the route from **10** to **2** was not pursued. However, when the coordinates of the $\pi$-bound vinylidene were perturbed, reoptimization resulted in **2**. The B3LYP/BS1-optimized geometries of $\mathbf{TS_{Ia\text{-}10}}$ and **10** are included in the Supporting Information.

**Pathway 2.** In the second pathway (orange curve), the $\sigma$-$C_1''$−H″ bond interacts with the rhodium, which facilitates H″ migration from $C_1''$ to $C_2''$. In the initial step, which has an enthalpic barrier of 12.9 kcal·mol$^{-1}$, the $\pi$-bound HCCPh ligand of **Ia** slips to bind to the rhodium through the $\sigma$-$C_1''$−H″ bond, forming intermediate **11**, which is endothermic and endergonic by 4.7 and 1.7 kcal·mol$^{-1}$. In this transformation the Rh−$C_1'$ bond shortens slightly in $\mathbf{TS_{Ia\text{-}11}}$ before returning to a similar value in **11**. Likewise, the Rh−$C_1''$ bond shortens with isomerization while the $C_1''$−H″ bond lengthens. In this $\sigma$-complex (**11**) the phenyl ring of the HCCPh ligand has rotated to align parallel with the Rh−P axes; this rotation takes place after $\mathbf{TS_{Ia\text{-}11}}$. The optimized geometries of $\mathbf{TS_{Ia\text{-}11}}$ and **11** are shown in Figure 5.

Species **11** is connected to **2** by $\mathbf{TS_{11-2}}$, which is characterized by the inverted T-shaped geometry and involves Rh−$C_1''$ bond formation and H″ migration to $C_2$. The alkynyl moiety is nearly linear, as the $C_1''$−$C_2''$−$C_{Ph}$ angle is ∼178°, and the phenyl ring is also aligned parallel with the Rh−P axes. Relative to **11**, the enthalpic and free energy barriers of this TS are 19.9 and 23.9 kcal·mol$^{-1}$, respectively.

We verified that $\mathbf{TS_{11-2}}$ connects **11** and **2** by following the intrinsic reaction coordinate (IRC) in both directions from

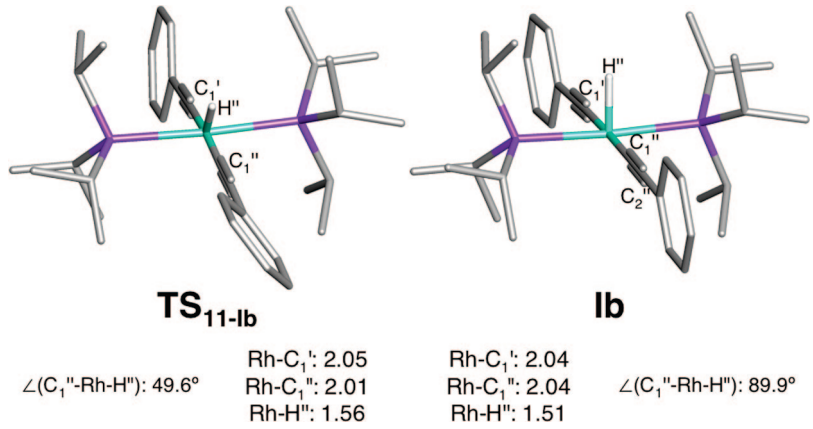


**Figure 7.** B3LYP/BS1-optimized geometries and select optimized parameters of $\mathbf{TS_{11\text{-}Ib}}$ and **Ib**. Distances listed are in angstroms and angles in degrees. Nonessential hydrogen atoms have been removed for clarity.

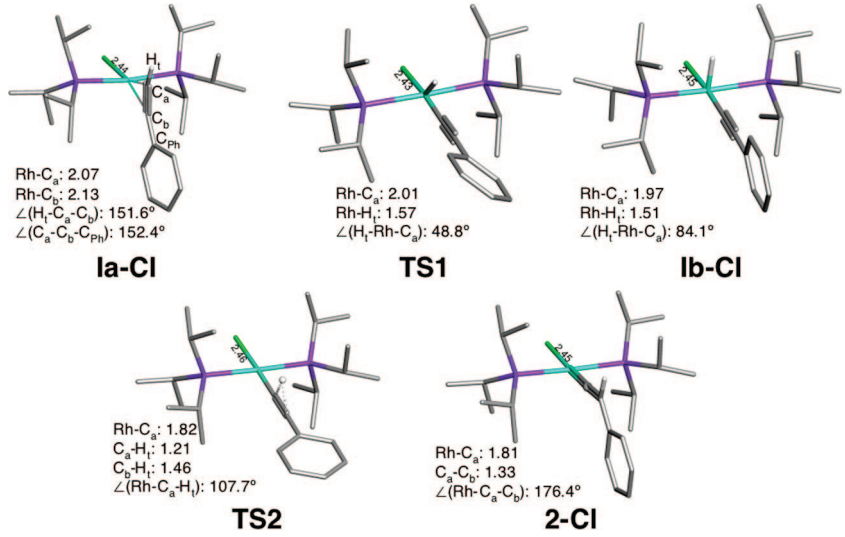


**Figure 8.** Optimized geometries (B3LYP/BS1) of **Ia-Cl**, **TS1**, **Ib-Cl**, **TS2**, and **2-Cl**. Select optimized bond lengths are included and are in angstroms. Nonessential hydrogen atoms have been removed for clarity.

**Table 4. Relative Enthalpies and Free Energies of the Analogues of Chlorine (energies are relative to Ia-Cl and are in kcal·mol$^{-1}$)**

| | relative energies | |
|---|---|---|
| species | $\Delta H^{\circ/\ddagger}$ | $\Delta G^{\circ/\ddagger}$ |
| **Ia-Cl** | 0 | 0 |
| **TS1** | 5.22 | 2.97 |
| **Ib-Cl** | 0.01 | −5.16 |
| **TS2** | 25.42 | 19.50 |
| **2-Cl** | −6.67 | −9.64 |

$\mathbf{TS_{11-2}}$.[25] In particular, the values of the Rh−H″ and $C_1''$−H″ distances and the Rh−$C_1''$−H″ angle in the coordinates of the last IRC optimization step for hydrogen migration to the rhodium, **A** (Figure 6), are very similar to those of **11**. A full optimization of the coordinates of **A** resulted in **11**. In following the vector for migration to $C_2''$ (**B**), the $C_2''$−H″ bond begins to form (1.14 Å) and the Rh−$C_1''$−H″ angle widens to 123.0°, which is ∼33° wider than the value in $\mathbf{TS_{11-2}}$. Likewise, the $C_1''$−$C_2''$−$C_{Ph}$ angle begins to bend. The IRC optimization terminates here as the phenyl ring begins to rotate to its position in **2**. The optimized geometries of $\mathbf{TS_{11-2}}$, **A**, and **B** are shown in Figure 6.

(25) (a) Gonzalez, C.; Schlegel, H. B. *J. Chem. Phys.* **1989**, *90*, 2154–2161. (b) Gonzalez, C.; Schlegel, H. B. *J. Phys. Chem.* **1990**, *94*, 5523–5527.

**Pathway 3.** The third pathway (blue) begins with the first step in pathway 2 (**Ia** → **11**). However, from **11** the reaction proceeds to the experimentally observed bis-alkynyl rhodium hydride complex **Ib** by the oxidative cleavage of the $\sigma$-$C_1''$−H″ bond ($\mathbf{TS_{11\text{-}Ib}}$). Species **Ib** is isoenthalpic with **Ia** and is characterized by typical Rh−C and Rh−H bond lengths. Relative to **11**, the enthalpic and free energy barriers to oxidative cleavage of the $C_1''$−H″ ($\mathbf{TS_{11\text{-}Ib}}$) are small, at 0.7 and 0.4 kcal·mol$^{-1}$, respectively. The optimized geometries of $\mathbf{TS_{11\text{-}Ib}}$ and **Ib** are shown in Figure 7.

Hydrogen is transferred directly from the rhodium to $C_2''$ through $\mathbf{TS_{Ib\text{-}12}}$; however, this process is uphill by 35.4 kcal·mol$^{-1}$ and results in an unstable intermediate where the vinylidene ligand is weakly bound to the rhodium through the $C_2''$−H″ bond (**12**). Since the barrier to this coupling is large ($\mathbf{TS_{Ib-12}}$), the TS between **12** and **2** was not pursued. However, when the coordinates of the vinylidene ligand were perturbed, optimization resulted in **2**. The optimized geometries of $\mathbf{TS_{Ib-12}}$ and **12** are included in the Supporting Information.

**Chloride Analogues.** Because of the difference in the reaction described above in comparison to [ClRh(P*i*Pr$_3$)$_2$($\eta^2$-HCCH)],[11,12] we examined the mechanism for vinylidene formation with

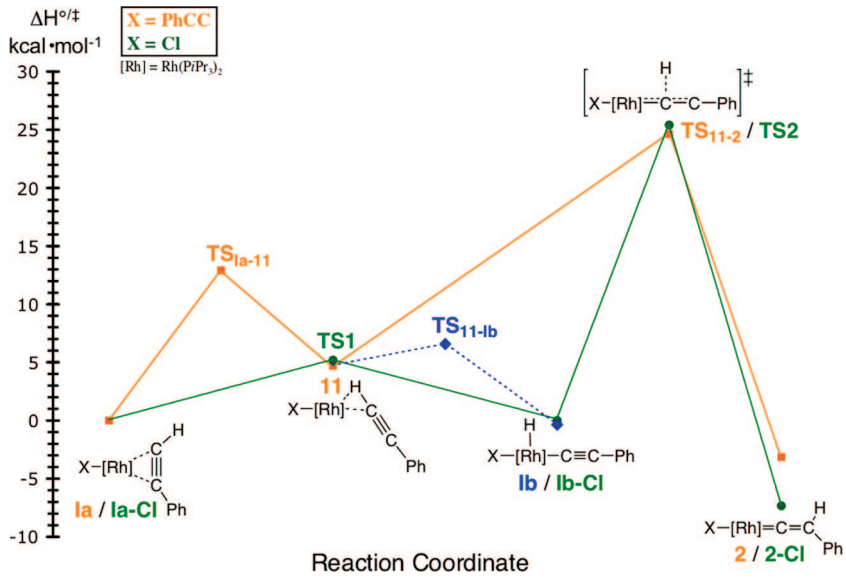


**Figure 9.** Comparison of the potential energy surfaces for the alkyne-to-vinylidene isomerization for the lowest energy pathways of X = alkynyl (orange) and of X = chloride (green). All the chloride species are new, and those intermediates closely related to the alkynyl species are labeled -Cl; i.e., the chloride species corresponding to **Ia** is **Ia-Cl**.

phenylacetylene adding *trans* to a chloride ion[26] rather than another phenylacetylene. The $\eta^2$-alkyne complex, TS for C−H bond cleavage, alkynyl rhodium hydride complex, TS for hydrogen migration, and vinylidene product are **Ia-Cl**, **TS1**, **Ib-Cl**, **TS2**, and **2-Cl**, respectively, which are analogues of **Ia**, $\mathbf{TS_{Ia-11}}$, **Ib**, $\mathbf{TS_{11-2}}$, and **2**, respectively. However, the analogue of **11** was not located. The optimized geometries of these species are shown in Figure 8, and the relative enthalpies and free energies of these species are presented in Table 4 (relative to **Ia-Cl**).

Geometrically, these species are very similar to their bis-alkynyl analogues. The $H_t-C_a-C_b$ and $C_a-C_b-C_{Ph}$ angles in **Ia-Cl** are similar to the analogous angles in **Ia**; however, the $Rh-C_a$ and $Rh-C_b$ distances are shorter than those in **Ia**. Species **TS1** exhibits a slightly shorter $Rh-H_t$ distance compared to the analogous distance in $\mathbf{TS_{11-Ib}}$, and the $H_t-Rh-C_a$ angle (48.8°) is slightly smaller. In **Ib-Cl**, the $Rh-H_t$ distance is identical to that of **Ib**, and the $Rh-C_a$ bond distance is once again slightly shorter. For **TS2**, the geometric parameters are very similar to those of $\mathbf{TS_{11-2}}$, and the relative orientation of the phenyl ring is the same between the two analogues. Likewise, the geometric parameters between **2-Cl** and **2** are also very similar, and the phenyl ring is aligned orthogonal to the Rh−P axes. The Rh−Cl distance is relatively insensitive to the entire reaction, less than the corresponding distance in the *trans* phenylacetylide.

The relative energies for most of these species are similar to the analogous energies of the bis-alkynyl system. The barrier to oxidative cleavage is once again small (**TS1**), and **Ia-Cl** is nearly isoenthalpic with **Ib-Cl**; however, the latter is exergonic by ∼4 kcal·mol$^{-1}$. Likewise, the enthalpic barrier of **TS2** is similar to that of $\mathbf{TS_{11-2}}$, but the free energy barrier is ∼6 kcal·mol$^{-1}$ lower in the former. The formation of **2-Cl** is more exothermic and exergonic than **2** by ∼3 and ∼4 kcal·mol$^{-1}$, respectively.

Mechanistically, this pathway is similar to pathway 2 for the bis-alkynyl system, but the analogue to the $\sigma$-bound HCCPh species (**11**) was not located. Instead, the first TS (**TS1**) results in oxidative cleavage of the C−H bond and direct formation of **Ib-Cl**. Species **TS2** connects **Ib-Cl** and **2-Cl** and is the TS for hydrogen migration and vinylidene formation. We verified that **TS2** connects **Ib-Cl** and **2-Cl** through IRC calculations. Several geometries from the IRC calculations when following the vector toward **Ib-Cl** were individually optimized, and all resulted in **Ib-Cl**. The lowest energy pathway for this isomerization in the bis-alkynyl system, pathway 2 (orange), is compared with this analogous chloro pathway (green) in Figure 9. The pathway for the formation of **Ib** is included in the figure (dashed, blue curve). The influence of the "spectator" ligand on the mechanism is dramatic. When a chloride ligand is *trans* to the isomerizing alkyne, the TS for alkyne isomerization ($\mathbf{TS_{Ia-11}}$), the $\sigma$-bound phenylacetylene intermediate (**11**), and the TS for oxidative C−H cleavage ($\mathbf{TS_{11-Ib}}$) "coalesce" into a single TS (**TS1**). On the other hand, when the phenylacetylide ligand is in the *trans* position, the $\sigma$-binding mode of the second phenylacetylene is stabilized. Instability of the $\sigma$-bound mode for the chloro analogue results in the lowest route to formation of the product beginning with **Ib-Cl** rather than with **11**.

## Conclusions

Initially, the allyl complex $[(\eta^3\text{-}C_3H_5)Rh(P\mathit{i}Pr_3)_2]$ (**1**) oxidatively adds one phenylacetylene and eliminates propene in a weakly exothermic step to form the first intermediate, $[(P\mathit{i}Pr_3)_2Rh(\eta^2\text{-}HCCPh)(CCPh)]$ (**Ia**). The preferred pathway to the final product, $[(P\mathit{i}Pr_3)_2Rh(CCPh)(CC(H)(Ph))]$ (**2**), is from the $\sigma$-bound HCCPh species $[(P\mathit{i}Pr_3)_2Rh(CCPh)(\sigma\text{-}HCCPh)]$ (**11**), which is an intermediate in the equilibrium between **Ia** and the bis-alkynyl rhodium hydride species $[(P\mathit{i}Pr_3)_2Rh(H)(CCPh)_2]$ (**Ib**). The formation of **Ib** is facile, but the system reverts to **11**, which is stabilized by a phenylacetylide ligand located *trans* to the $\sigma$-bound phenylacetylene ligand before forming **2**. This mechanism is reminiscent of other reactions that proceed to product from the less (least) stable intermediate.[27] Replacement of the *trans* phenylacetylide by chloride changes the mechanism to a

(26) The chloride was assigned the cc-pVDZ basis set. The other atoms were assigned the same basis sets as their bis-alkynyl analogues.

(27) (a) Chan, A. S. C.; Pluth, J. J.; Halpern, J. *J. Am. Chem. Soc.* **1980**, *102*, 5952–5954. (b) Halpern, J. *Science* **1982**, *217*, 401–407. (c) Landis, C. R.; Halpern, J. *J. Am. Chem. Soc.* **1987**, *109*, 1746–1754.

more common *1−3 shift* mechanism. Overall, the calculated barrier is still somewhat too high (4 to 6 kcal/mol) to explain the observed room-temperature rearrangement (**Ib** → **2**). Most likely this error is simply the result of the particular functional (B3LYP) used for these calculations.

The relative energies of **Ia**, **Ib**, and **2** are quite sensitive to the phosphine ligand; **2** is the product for weaker $\pi$-acids and **Ia** is preferred with stronger $\pi$-acids. Species **Ib** and **Ia** are isoenthalpic only with the P*i*Pr$_3$ ligands; other phosphines, even PEt$_3$, stabilize **Ia** over **Ib**. Thus, in any higher-level calculations the choice of phosphine will be critical.

**Acknowledgment.** This work was supported by grants from the NSF (CHE-0518074, CHE-0541587, and DMS-0216275), the Welch Foundation (A0648), and the Texas A&M University Supercomputing Facility.

**Supporting Information Available:** Optimized geometries for all species and the relative energies for the cobalt and iridium congeners of species **Ia** through **2**. This material is available free of charge via the Internet at http://pubs.acs.org.

OM8001137